ORIGINAL RESEARCH

Plasminogen Activator Inhibitor-1 Deficiency Augments Visceral Mesothelial Organization, Intrapleural Coagulation, and Lung Restriction in Mice with Carbon Black/Bleomycin–Induced Pleural Injury

Torry A. Tucker[1], Ann Jeffers[1], Alexia Alvarez[1], Shuzi Owens[1], Kathleen Koenig[1], Brandon Quaid[1], Andrey A. Komissarov[1], Galina Florova[1], Hema Kothari[2], Usha Pendurthi[2], L. Vijaya Mohan Rao[2], and Steven Idell[1]

[1]The Texas Lung Injury Institute, [2]Department of Cellular and Molecular Biology, University of Texas Health Science Center at Tyler, Tyler, Texas

Abstract

Local derangements of fibrin turnover and plasminogen activator inhibitor (PAI)-1 have been implicated in the pathogenesis of pleural injury. However, their role in the control of pleural organization has been unclear. We found that a C57Bl/6j mouse model of carbon black/bleomycin (CBB) injury demonstrates pleural organization resulting in pleural rind formation (14 d). In transgenic mice overexpressing human PAI-1, intrapleural fibrin deposition was increased, but visceral pleural thickness, lung volumes, and compliance were comparable to wild type. CBB injury in PAI-$1^{-/-}$ mice significantly increased visceral pleural thickness ($P < 0.001$), elastance ($P < 0.05$), and total lung resistance ($P < 0.05$), while decreasing lung compliance ($P < 0.01$) and lung volumes ($P < 0.05$). Collagen, α-smooth muscle actin, and tissue factor were increased in the thickened visceral pleura of PAI-$1^{-/-}$ mice. Colocalization of α-smooth muscle actin and calretinin within pleural mesothelial cells was increased in CBB-injured PAI-$1^{-/-}$ mice. Thrombin, factor Xa, plasmin, and urokinase induced mesothelial–mesenchymal transition, tissue factor expression, and activity in primary human pleural mesothelial cells. In PAI-$1^{-/-}$ mice, D-dimer and thrombin–antithrombin complex concentrations were increased in pleural lavage fluids. The results demonstrate that PAI-1 regulates CBB-induced pleural injury severity via unrestricted fibrinolysis and cross-talk with coagulation proteases. Whereas overexpression of PAI-1 augments intrapleural fibrin deposition, PAI-1 deficiency promotes profibrogenic alterations of the mesothelium that exacerbate pleural organization and lung restriction.

Keywords: plasminogen activator inhibitor-1; coagulation; plasmin; thrombin; mesothelial–mesenchymal transition

Clinical Relevance

Plasminogen activator inhibitor (PAI) deficiency contributes to the progression of pleural injury. The lack of PAI-1 augments fibrinolytic and coagulation protease activity and paradoxically exacerbates injury.

Pleural fibrosis can result in restrictive lung disease and clinically significant dyspnea associated with fibrothorax. Common causes of fibrothorax are empyema or pneumonia with undrained complicated parapneumonic effusion, tuberculosis, collagen vascular diseases, trauma and hemothorax, post–coronary artery bypass surgery, and asbestos-related pleural disease (1). Fibrothorax contributes to the increased mortality in patients with parapneumonic effusions/empyema and comorbidities (2). About 80,000 United States and United Kingdom patients with empyema or complicated parapneumonic

(Received in original form July 1, 2013; accepted in final form September 4, 2013)

This work was supported by National Institutes of Health grant HL115466 and the Texas Lung Injury Institute.

Author Contributions: T.A.T. designed research, performed research, analyzed data, and wrote the paper; A.J., A.A., S.O., K.K., B.Q., G.F., A.A.K., and H.K. performed research analyses; U.P. analyzed data and assisted with aspects of experimental design; L.V.M.R. provided vital reagents and analyzed data, and assisted with aspects of experimental design; and S.I. designed research, analyzed data, and wrote the paper with T.A.T., and reviewed all drafts of the work.

Correspondence and requests for reprints should be addressed to Torry A. Tucker, Ph.D., the Texas Lung Injury Institute, the University of Texas Health Science Center at Tyler, 11937 U.S. Highway 271, Biomedical Research Building, Laboratory C-5, Tyler, TX 75708. E-mail: torry.tucker@uthct.edu

This article has an online supplement, which is accessible from this issue's table of contents at www.atsjournals.org

Am J Respir Cell Mol Biol Vol 50, Iss 2, pp 316–327, Feb 2014

Originally Published in Press as DOI: 10.1165/rcmb.2013-0300OC on September 11, 2013
Internet address: www.atsjournals.org

pleural effusions annually require pleural drainage in an effort to treat pleural sepsis and prevent lung restriction due to fibrothorax (3). Many more develop pleural loculation and fibrosis in association with malignancy (3). Although plasminogen activator inhibitor (PAI)-1 has been implicated in the pathogenesis of pleural organization and poor outcomes of pleural injury, its role at present has been strictly ascribed to suppression of intrapleural fibrinolysis (4).

Disordered fibrin turnover has likewise long been associated with acute lung injury and interstitial lung diseases, including idiopathic pulmonary fibrosis. In these diseases, decreased fibrinolytic activity of lung lavage fluids is characteristic, and is attributable to an increase of PAI-1 (5). Prior studies have shown that PAI-1 deficiency was protective against bleomycin-induced pulmonary fibrosis (6, 7), whereas lung fibrosis was exacerbated in plasminogen and plasminogen activator–deficient mice (8). Increased PAI-1 has previously been shown to increase pleural loculation in relatively acute pleural injury (over 4–5 d) (9), but its effect on pathophysiologic lung restriction and fibrothorax has not, to our knowledge, been previously studied.

Pleural injury is characterized by the proliferation of α-smooth muscle actin (α-SMA)–expressing myofibroblasts (10, 11). These cells promote the accumulation of extracellular matrix (ECM) proteins, including collagen (Col)-1 (12). However, the source of myofibroblasts in evolving fibrothorax remains unclear. Pleural mesothelial cells (PMCs) have recently been shown to undergo a process called mesothelial–mesenchymal transition (MesoMT) (1, 13), which is similar to epithelial–mesenchymal transition (EMT). Although transforming growth factor (TGF)-β1 potently induces EMT, recent studies have shown that procoagulant proteases, such as factor Xa (FXa) and thrombin (THB), can also induce markers of EMT in lung epithelial cells (14, 15). These findings, and the abundance of procoagulants in exudative pleural effusions (15–17), suggest that these proteases have the potential to drive MesoMT in fibrosing pleural injury *in vivo*.

In this study, we introduce and characterize a model system of carbon black/bleomycin (CBB)-induced pleural fibrosis in C57Bl/6j mice, new techniques to harvest pleural lavage and culture primary PMCs, and new applications of computed tomography (CT) imaging and physiologic assessments to assess the role of PAI-1 in evolving fibrothorax. We now show that PAI-1 deficiency exacerbates CBB-induced pleural injury in mice, that the process involves cross-talk between PAI-1 and procoagulant responses in pleural fluids and tissues, and that coagulation proteases, two-chain urokinase plasminogen activator (uPA) and plasmin (PLN) can promote MesoMT that may contribute to pathophysiologic derangements of pulmonary function indicative of lung restriction in evolving fibrothorax.

Materials and Methods

Additional methods are described in the online supplement.

CBB Mouse Model

All experiments involving animals were approved by the Institutional Animal Care and Use Committee at the University of Texas Health Science Center at Tyler. Wild-type (WT) C57Bl/6j mice and PAI-$1^{-/-}$ mice and PAI-1 transgenic (PAI-1^{Tg}) mice on a C57Bl/6j background were purchased from Jackson Laboratory (Bar Harbor, Maine). The CBB mouse model of pleural fibrosis was established as previously described in CD1 mice (10), with some modifications. Isofluorane-anesthetized C57BL/6j mice were intrapleurally injected with 100 μl of a CBB mixture (0.1 mg carbon black [Degussa AG, Frankfurt, Germany]/0.07 U bleomycin [Teva Parenteral Medicines, Irvine, CA]) prepared in 0.9% saline. Control animals were intrapleurally injected with 100 μl of 0.9% saline. Pleural injury was then allowed to progress for 7, 14, or 21 days, at which point the mice were killed.

Measurement of Pulmonary Function Tests

Pulmonary function tests were performed immediately before CT imaging and before mice were killed, as previously described (18). Briefly, mice were anesthetized with a ketamine/xylazine mixture. Anesthetized mice were next intubated by inserting a sterile, 20-gauge intravenous canula through the vocal cords into the trachea. Elastance, compliance, and total lung resistance measurements were then collected using the flexiVent system (SCIREQ, Tempe, AZ). The "snapshot perturbation method" was used to study lung function in the CBB injury model. This method measures total lung resistance, compliance, and elastance of the entire respiratory system. Increased total lung resistance in the CBB model may reflect lung contraction associated with pleural rind formation with concurrent distortion of the airways. The flexiVent was set to a tidal volume of 30 ml/kg at a frequency of 150 breaths/min against 2–3 cm H_2O positive end-expiratory pressure, according to manufacturer's specifications. The mice were maintained under anesthesia using isofluorane throughout the pulmonary function testing.

CT Scans and Measurements of Lung Volume

After ketamine/xylazine injection, mice were anesthetized further using an isoflurane/O_2 mixture to ensure that mice remained deeply anesthetized and to minimize spontaneous breaths. The Explore Locus Micro-CT Scanner (General Electric, GE Healthcare, Wauwatosa, WI) was used for CT imaging. CT scans were performed during full inspiration and at a resolution of 93 μm. Lung volumes were calculated from lung renditions collected at full inspiration. Microview software was used to analyze lung volumes and render three-dimensional images.

Phase Contrast Microscopy

Phase contrast microscopy was used to document phenotypic changes in PMCs exposed to selected agonists.

Flow Cytometry

PMCs were first isolated from saline- and CBB-treated WT mice by tryptic wash. Isolated cells were then washed, fixed with 2% buffered formalin, and permeabilized with 0.1% saponnin. Cells were then labeled for α-SMA (Alexafluor 488; R&D Systems, Minneapolis, MN) and calretinin (DyLight 649; Sigma-Aldrich, St. Louis, MO), and analyzed on a Guava easyCyte flow cytometer (Millipore, Billerica MA).

Statistical Analysis

All statistics were performed using the Mann-Whitney *t* test. A *P* value of less than 0.05 was considered significant.

Results

α-SMA Expression Localizes to the Mesothelium and Is Increased in Pleural Tissue from Patients with Pleuritis versus Patients with Morphologically Normal Pleura

We first sought to determine if myofibroblasts were detectable in human lung sections from patients diagnosed as having nonspecific pleuritis. Lung sections from histologically normal subjects and those with pleuritis were immunofluorescently labeled and pleural linings compared. Calretinin is a mesothelial cell–specific marker in the lung, and was used to detect PMCs in lung tissue sections (13, 19). Calretinin was found in the mesothelium of both normal and pleuritis lung tissues. α-SMA, however, was only detected in the mesothelium and submesothelium of pleuritis tissues (Figure 1A). Furthermore, α-SMA and calretinin colocalized in human pleuritis tissues. These findings show that nonspecific human lung pleuritis is characterized by the presence of myofibroblasts, which are absent in normal human pleural tissues, and that PMCs may contribute to the myofibroblast population. We next compared tissue sections from the same patients for the presence of ECM proteins, including fibrin and collagen. As expected, pleuritis tissues consistently exhibited robust fibrin and collagen deposition at the level of the mesothelium and within the subpleural tissues (Figure 1B).

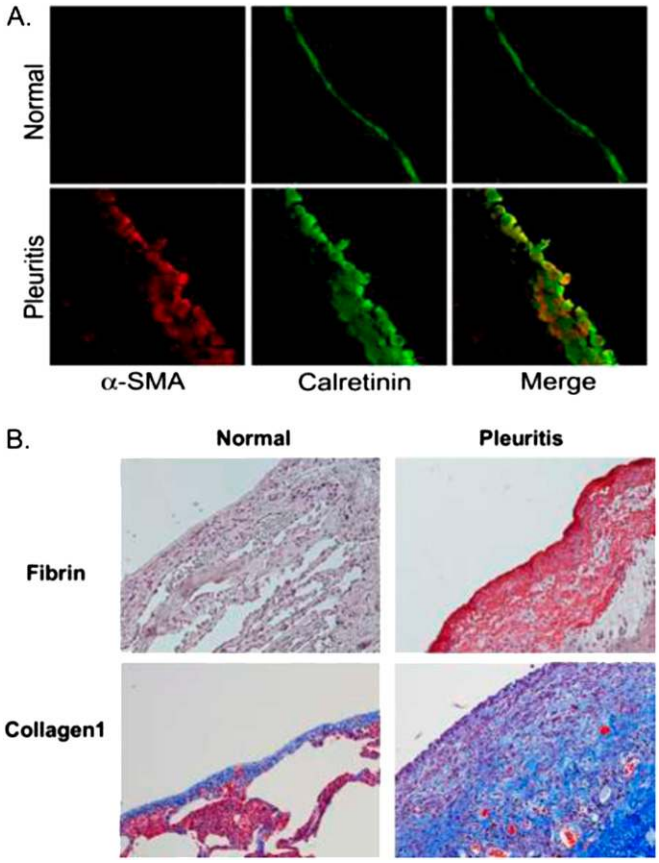

Figure 1. Tissue colocalization of α-smooth muscle actin (α-SMA) and calretinin in human pleuritis lung. Tissue sections were prepared from the lungs of normal subjects and patients with nonspecific pleuritis (n = 3/group). (*A*) The sections were then probed for the expression of α-SMA (*red*) and calretinin (*green*) by the pleural mesothelium lining using immunofluorescence. The sectioned pleural mesothelium in its entirety was analyzed for α-SMA and calretinin expression. All images were taken at 40× magnification on a confocal microscope. (*B*) Tissue sections from normal subjects and patients with nonspecific pleuritis were probed for fibrin via immunohistochemistry and collagen via Trichrome stain. The sectioned pleural mesothelium in its entirety was analyzed for fibrin deposition (*red stain*). Tissue sections from normal subjects and patients with pleuritis were analyzed for collagen deposition (*blue*). All images were taken at 20× magnification on a Nikon Eclipse Ti inverted microscope (Nikon, Dallas, TX). Illustrated findings are representative of three sections per group.

CBB Injury Induces Pleural Fibrosis in Mice

Because intrapleural administration of a CBB mixture has previously been shown to cause pleural fibrosis in CD1 mice (10), we next sought to establish a model of pleural fibrosis in C57Bl/6j mice. The left hemithoraces of C57Bl/6j mice were intrapleurally injected with saline or a CBB mixture in saline. Treated animals were then analyzed 7, 14, and 21 days after injection. Animals were anesthetized and CT scan analyses were performed on saline- and CBB-treated mice. Three-dimensional lung renditions were then constructed from the CT scans and lung volumes were calculated, which showed that CBB-mediated lung injury preferentially localizes to the left hemithorax, but that both hemithoraces were affected (Figure 2A). These data indicate that CBB induces pleural injury that is readily detected by CT scanning, and restricts lung volumes within 14 days in C57Bl/6j mice.

α-SMA–Expressing Cells Are Associated with and Enriched in CBB-Mediated Pleural Thickening

Because previous reports have shown that myofibroblasts are represented in the thickened pleura of CBB-injured CD1 mice (10), we next tested lung sections from saline- and CBB-treated mice for α-SMA by immunohistochemistry (IHC). We found that α-SMA expression appeared in the injured lung pleura as early as 7 days in this model, and increased within the pleural rind over 21 days (Figure 2B). These findings support the concept that myofibroblasts contribute to morphologic and pathophysiologic derangements associated with CBB-induced pleural injury.

CBB-Induced Pleural Injury Is Associated with Extravascular Fibrin and Collagen Deposition

Because the pleural cavities from CBB-treated mice appeared to be encased in a transitional neomatrix, tissue sections were assayed for fibrin(ogen) by IHC. Fibrin-related staining was confirmed at 7-, 14-, and 21-day time points; however, fibrin antigen was highest at 7 days after CBB

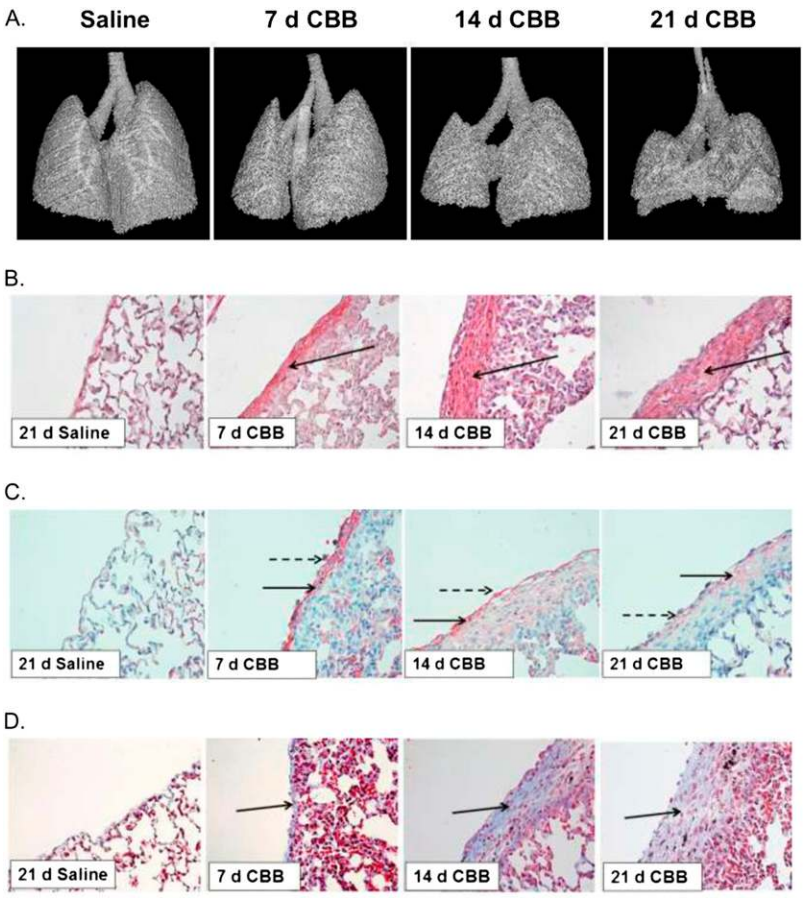

Figure 2. Computed tomography (CT) scan analysis of carbon black/bleomycin (CBB)-injured pleural cavities in mice. Saline- and CBB-injured mice were analyzed by CT scan 7, 14, and 21 days after CBB or saline injection. (*A*) Three dimensional (3D) reconstructions from CT scans illustrate altered lung morphology after induction of CBB pleural injury. The 3D renderings are representative of the findings of all animals in each group consisting of four to six animals per group. (*B*) Lung sections from 7-, 14-, and 21-day CBB-injured and saline-challenged mice were stained for α-SMA by immunohistochemistry. α-SMA expression increased throughout the 21-day time course in the visceral lung pleura in CBB-injured mice. *Solid arrows* indicate areas of α-SMA positivity. α-SMA expression of the mesothelium was absent in the 21-day saline-treated samples. (*C*) Lung tissue sections from saline- and CBB-injured mice were immunohistochemically stained for fibrin(ogen). Fibrin(ogen) staining (*red*) is most prominent at the pleural surface by 7 days, and attenuates over the 21-day time course. *Solid arrows* indicate areas of fibrin deposition. *Dashed arrows* indicate the presence of cells within the fibrin matrix (30 fields/section for each of 3 mice/group) were analyzed to determine fibrin deposition. (*D*) Lung tissue sections were Trichrome stained to detect collagen deposition (*blue*) over the 21-day time course after intrapleural saline or CBB administration. Collagen deposition became prominent by 14 days and remained so through 21 days (30 fields/section for each of 3 mice/group) were analyzed to determine collagen deposition. Trichrome-stained sections were also used to analyze pleural thickness. Mesothelial and subpleural thickening was apparent by 7 days, and progressively worsened over the 14- and 21-day period (30 fields/section for each of 3 mice/group).

administration (Figure 2C). No fibrin was detected in saline controls. PMCs appeared to be trapped in the fibrin mesh, which encapsulated the injured lungs (Figure 2C).

Collagen deposition was next assayed by Trichrome and picrosirius staining. The saline controls displayed little-to-no collagen at the level of the pleural mesothelium throughout the time course. CBB-injured lungs exhibited increased Trichrome staining in the lung pleura by 7 days, which progressively increased over the 21 days (Figure 2D). CBB-induced collagen expression in the submesothelial tissue was greatest at 21 days, and was limited to the pleural and subpleural layers. Collagen detection by Trichrome staining was confirmed by picrosirius staining, which showed a progressive increase in collagen deposition in the pleural mesothelium from 7 through 21 days (data not shown). These findings suggest that the neomatrix associated with CBB-mediated injury incorporates detectable fibrin deposition by 2 days, which is gradually infiltrated by collagen over 21 days. Histologic assessment of Trichrome-stained lung sections showed that CBB injury increased visceral pleural thickening, which was progressive over 21 days (Figure 2D). The parietal pleural surfaces exhibited mild pleural thickening (data not shown). These findings indicate that CBB injury elicits progressive fibroproliferation over 21 days.

PMCs Contribute to the Pleural Myofibroblast Population in CBB Pleural Injury

Because the myofibroblasts associated with CBB injury appeared to localize to the pleural and subpleural mesothelium, as detected by IHC, we next sought to confirm the findings using confocal microscopy to detect colocalization of calretinin and α-SMA in CBB-induced pleural injury. Saline-treated mouse lung tissues were positive for calretinin (*green*) at the surface of the pleural mesothelium, but were negative for α-SMA (*red*) (Figure 3A). Conversely, CBB-treated lung sections were positive for both calretinin and α-SMA at the level of the mesothelial and submesothelial layer with colocalization of the markers, indicated by an orange–yellow color on merged images.

In a complimentary approach, cells isolated by tryptic pleural lavage of 14 days saline- and CBB-injured WT mice were labeled for calretinin and α-SMA and analyzed by flow cytometry (Figure 3B). Flow analyses showed that greater than 80% of the cells isolated from pleural cavity were positive for calretinin, indicating that they are mesothelial in origin. Although 18% of the assayed cells were positive for α-SMA, the vast majority (>95%) of the α-SMA^{+} cells were also positive for calretinin. These findings buttress the concept that PMCs contribute to the population of visceral pleural myofibroblasts in CBB injury.

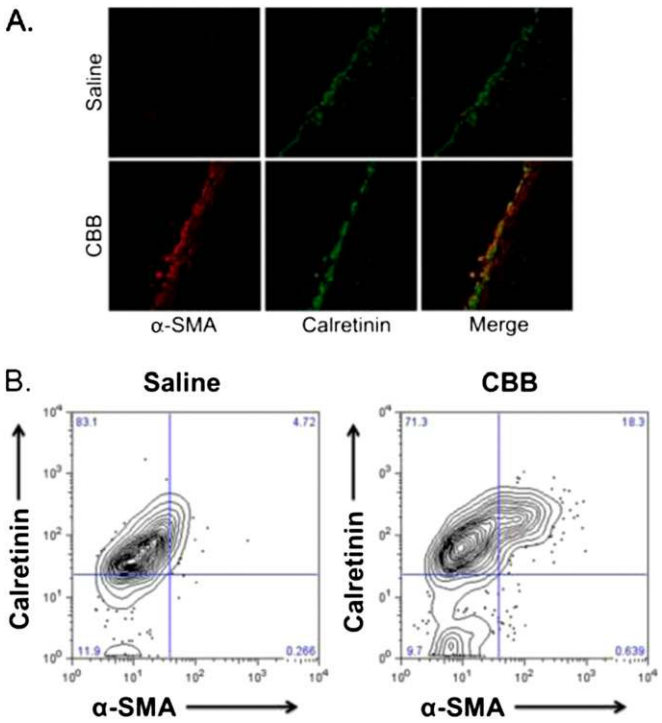

Figure 3. α-SMA and calretinin expression are colocalized in CBB-injured lung mesothelium. (*A*) Tissue sections were prepared from the lungs of saline- and CBB-injured mice at 14 days. The sections were then probed for the expression of α-SMA (*red*) and calretinin (*green*) by the pleural mesothelium lining using immunofluorescence. The sectioned pleural mesothelium in its entirety was analyzed for colocalization of α-SMA and calretinin expression. All images were taken at 40× magnification on a confocal microscope (n = 3 mice/group analyzed). (*B*) Cells isolated from the pleural cavity of 14-day saline- and CBB-treated mice were immunofluorescently colabeled for the myofibroblast marker, α-SMA (Alexafluor 488), and the mesothelial cell marker, calretinin (DyLight 649), and plotted to show cosegregation of a double-positive cell population. Representative findings from three mice per group are illustrated.

PAI-1 Deficiency Contributes to More Severe Lung Restriction in CBB-Induced Pleural Injury

The contribution of PAI-1 to the pathogenesis of visceral pleural thickening and lung restriction was next investigated. WT, PAI-$1^{-/-}$, and PAI-1^{Tg} mice were injected with CBB or saline and monitored over 14 days. CT analyses showed that CBB-mediated injury significantly reduced lung volumes in WT and PAI-$1^{-/-}$ mice compared with the saline control animals ($P < 0.05$ and $P < 0.01$, respectively; Figure 4A). Although there was a trend toward significance, CBB-treated PAI-1^{Tg} mice did not demonstrate significantly lower lung volumes than saline control animals at 14 days. Conversely, CBB injury significantly reduced lung volumes in PAI-$1^{-/-}$ mice when compared with CBB-treated WT and PAI-1^{Tg} mice ($P < 0.05$ and < 0.01, respectively). Pulmonary function testing showed that lung resistance was significantly increased by CBB-mediated injury in WT, PAI-$1^{-/-}$, and PAI-1^{Tg} mice ($P < 0.01$, $P = 0.01$; Figure 4B), which may, at least in part, be attributable to airway distortion associated with development of pleural rind formation and lung contraction. Furthermore, CBB-injured PAI-1–deficient animals exhibited significantly higher resistance than CBB-injured WT and PAI-1^{Tg} mice ($P = 0.02$). CBB injury significantly increased elastance in WT, PAI-$1^{-/-}$, and PAI-1^{Tg} ($P < 0.01$; Figure 4C) and decreased compliance ($P <$ 0.01 in WT, PAI-$1^{-/-}$, and PAI-1^{Tg} mice; Figure 4D). CBB-treated PAI-$1^{-/-}$ mice demonstrated significantly higher elastance ($P < 0.01$) and significantly lower compliance compared with similarly treated WT and PAI-1^{Tg} mice at 14 days ($P = 0.02$ and 0.04, respectively; Figure 4D). These data indicate that PAI-1 deficiency contributes to more severe restriction in CBB-injured versus WT or control mice at 14 days.

PAI-1–Deficient Mice Exhibit Increased Pleural Organization Compared with WT Mice

To relate histological derangements associated with CBB-induced injury to the pathophysiologic findings, we next performed Trichrome staining on lung sections from WT, PAI-$1^{-/-}$, and PAI-1^{Tg} mice. PAI-$1^{-/-}$ mice also elaborated more submesothelial collagen versus WT and PAI-1^{Tg} mice (Figure 4E). All groups exhibited significant pleural thickening after CBB injury compared with the saline control animals ($P < 0.01$; Figure 4E). PAI-$1^{-/-}$ mice exhibited significantly increased pleural thickening versus WT and PAI-1^{Tg} mice after CBB treatment at 14 days ($P < 0.01$). Gross analysis of CBB injury at 14 days showed clearly worse injury in PAI-$1^{-/-}$ mice. CBB-injured PAI-1^{Tg} animals exclusively demonstrated fibrinous strands in the pleural cavity (data not shown). Tissue sections from 14-day CBB-injured WT, PAI-$1^{-/-}$, and PAI-1^{Tg} mice were next stained for fibrin(ogen) by IHC. Although WT, PAI-$1^{-/-}$, and PAI-1^{Tg} mice were positive for pleural fibrin (ogen) antigen after CBB injury at 14 days (Figure 4F), PAI-1^{Tg} mice exhibited significantly thicker fibrin(ogen) containing pleural rinds than WT or PAI-$1^{-/-}$ mice (Figure 4G). Although previous reports showed that PAI-1 deficiency contributes to increased activation of TGF-β (20, 21), total and active pleural lavage TGF-β levels were not significantly different between WT and PAI-$1^{-/-}$ mice with or without CBB-induced pleural injury (range of total TGF-β, 1.5 ± 0.7 ng/ml; range of active TGF-β, 67 ± 22 pg/ml) at 14 days (n = 4–6 mice/group, data not shown), nor were any different trends apparent at 2, 7, or 21 days (n = 3 mice/group). These data suggest that PAI-1 deficiency in the aggregate contributes to worse visceral pleural organization after CBB-induced injury, and suggests that the effects are not attributable to detectable robust upstream increments in TGF-β activity.

CBB-Injured PAI-1–Deficient Mice Exhibit Increased Pleural Lavage Active PLN, D-Dimer Concentrations, and THB–Antithrombin Complexes

To determine PAI-1 levels in saline- and CBB-injured mice, pleural lavages from WT, PAI-$1^{-/-}$, and PAI-1^{Tg} mice were assayed for PAI-1 by ELISA. CBB injury

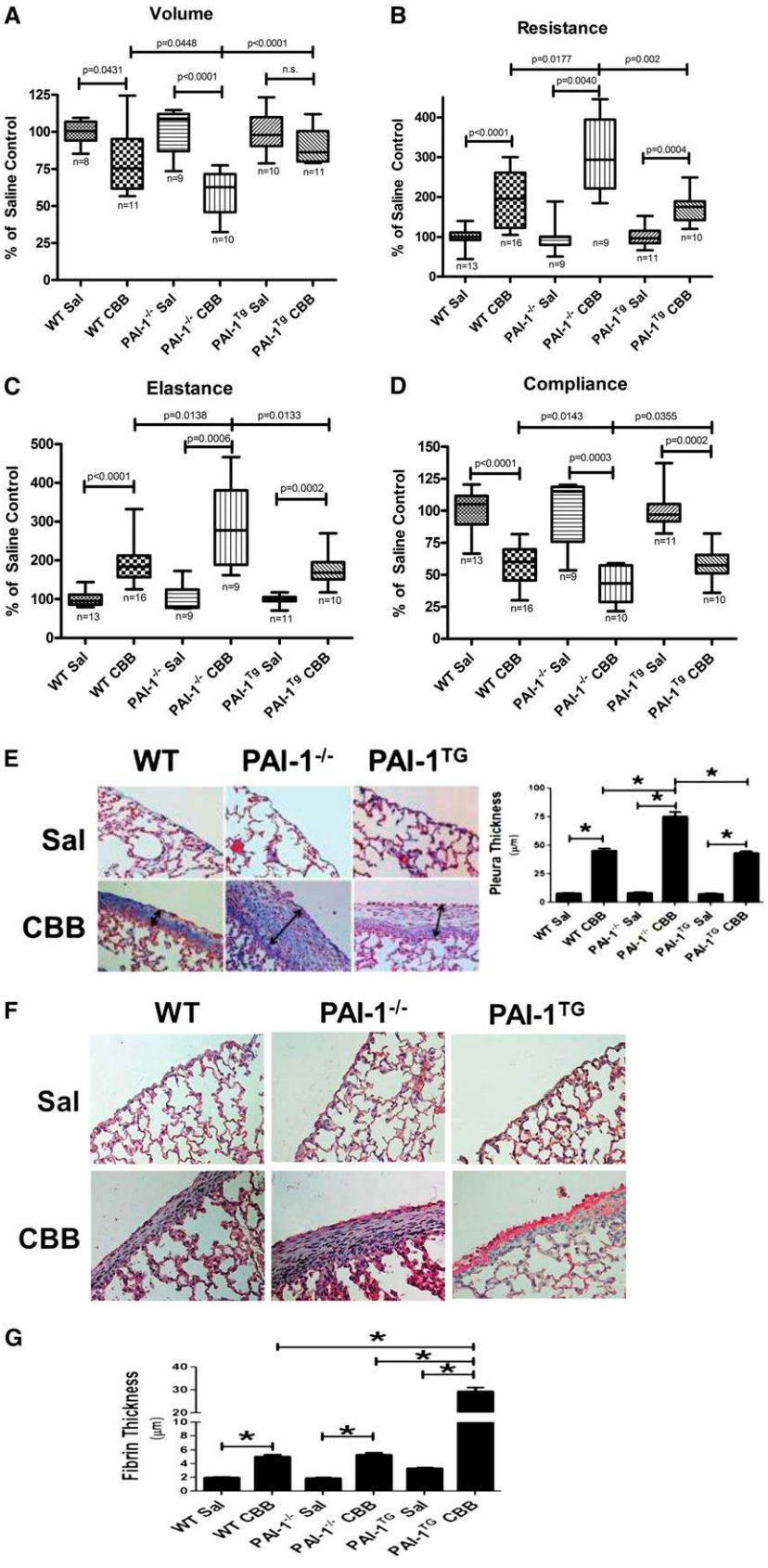

Figure 4. (See figure legend on following page.)

significantly increased PAI-1 levels in WT mice. As expected, PAI-1 levels were undetectable in PAI-1–deficient animals, whereas PAI-1^{Tg} mice expressed significantly more basal PAI-1 than WT animals (*see* Figure E1 in the online supplement). Because PAI-1 was elevated in pleural lavage of CBB-injured WT mice, we next assessed changes in active PLN (Figure 5A). CBB injury significantly decreased active PLN in pleural lavage of WT mice. Conversely, active PLN was significantly increased in CBB-injured PAI-$1^{-/-}$ compared with WT mice. Increased active PLN levels in saline-treated PAI-$1^{-/-}$ versus WT mice were not significantly different, but were consistent with previously published studies (22, 23). Consistent with these findings, pleural lavage D-dimers (Figure 5B) were significantly increased in CBB-injured PAI-$1^{-/-}$ and PAI-1^{Tg} mice, and were significantly increased in the PAI-1–deficient animals versus the WT CBB-injured mice ($P = 0.03$). Analyses of pleural lavages over a 21-day time course showed that D-dimers were consistently higher in CBB-injured PAI-$1^{-/-}$ mice. D-dimer levels were highest at 2 days, and steadily decreased throughout the time course ($n = 3$ mice/group at each interval; Figure E2A). Because FXa activity in pleural lavages from saline- and CBB-treated mice was generally below the detectable range by amidolytic analyses, a THB–antithrombin (TAT) ELISA was performed. CBB-injured mice demonstrated increased TAT complexes compared with saline control animals (Figure 5C), but the levels were not significantly different. Furthermore, CBB-injured PAI-$1^{-/-}$ mice demonstrated significantly higher levels of pleural lavage TAT complexes than CBB-treated WT and PAI-1^{Tg} mice at the 14-day interval ($P = 0.05$ and 0.01, respectively). In a 21-day time course, TAT complexes were consistently higher in CBB-injured PAI-$1^{-/-}$ mice than in other groups ($n = 3$ mice/group at each interval; Figure E2B). These data clearly indicate that pleural lavage procoagulant activity was most increased in CBB-injured PAI-$1^{-/-}$ mice. Because TAT concentrations were elevated in CBB-injured mice, tissue factor (TF) expression was assayed by IHC. CBB-injured mice demonstrated elevated TF antigen at the mesothelial surface. PAI-$1^{-/-}$ mice expressed significantly more TF antigen than similarly treated WT mice

(Figure 5D). These findings suggest that increased TF expression and activity *in vivo* maintains WT levels of pleural fibrin in PAI-1$^{-/-}$ mice (Figure 4G) despite increased intrapleural fibrinolytic activity (Figure 5B).

Increased Appearance of α-SMA–Expressing PMCs in PAI-1–Deficient Mice

Immunofluorescence colocalization assays were next performed, and showed colocalization of calretinin (*green*) and α-SMA (*red*) in the mesothelium and submesothelial tissues of WT animals, and was increased in PAI-1$^{-/-}$ mice (Figure 6).

Coagulation Cascade and Fibrinolytic Pathway Proteases Drive MesoMT *In Vitro*

Because pleural mesenchymal markers, fibrin(ogen) deposition, pleural lavage TAT complexes, and D-dimer levels were increased in PAI-1–deficient mice, we next interrogated the role of the coagulation cascade proteases, uPA and PLN, on MesoMT *in vitro*. Serum-starved human PMCs (HPMCs) were treated with TGF-β (positive control), FXa, THB, uPA, and PLN for 48 hours and assayed for markers of MesoMT and TF. TGF-β induced α-SMA, Col-1, and PAI-1 expression in HPMCs (Figure 7A). FXa, THB, PLN, and uPA induced α-SMA expression in HPMCs. Furthermore, TF expression was induced by FXa, THB, PLN, and uPA in HPMCs. Col-1, which is detected as two bands with molecular weights around 130 and 140 kD, representing the α1 and α2 isoforms, was induced by FXa, PLN, and uPA. Similar results were found in murine PMCs treated with TGF-β, FXa, THB, PLN, and uPA (data not shown). Because phosphoinositide 3-kinase/Akt signaling has been implicated in the mesenchymal transition of peritoneal mesothelial cells (24), Akt phosphorylation was also evaluated. TGF-β, FXa, THB, PLN, and uPA induced Akt phosphorylation in PMCs.

The increased expression of Col-1, α-SMA, and TF in HPMCs was confirmed by PCR analyses (Figure 7B; primer sequences for PCR analyses are found in (Table 1). TGF-β significantly increased Col-1 mRNA, whereas FXa, THB, PLN, and uPA showed increasing trends that were not significant (Figure 7B1). α-SMA mRNA was significantly increased by TGF-β, FXa, and THB. The same incremental trends of α-SMA mRNA were observed with PLN and uPA treatment, but did not reach significant levels. All treatments, including uPA and PLN, induced α-SMA protein (Figure 7A). TF expression was significantly induced by these same stimuli, with the exception of TGF-β and PLN (Figure 7B) (2). Although PLN treatment increased TF mRNA levels, the changes were not statistically significant. Phenotypic changes indicative of mesenchymal change (cellular elongation) were also observed within 48 hours of treatment with TGF-β, FXa, THB, PLN, and uPA of HPMCs (Figure 7C). In additional dose-ranging studies, HPMCS were treated with THB (13–0.7 nM; Figure 7D) and PLN (6–0.3 nM; Figure 7E) for 48 hours and then tested for markers of MesoMT. THB induced α-SMA, Akt phosphorylation, and PAI-1 expression over the full range of doses. With the exception of the highest-dose THB (13 nM, which presumably cleaved the product), THB (7–0.7 nM) induced Col-1 protein. Exposure to THB or PLN at all doses increased TF expression in HPMCs. PLN induced markers of MesoMT (Col-1, PAI-1, and α-SMA) at all concentrations except at the lowest dose (0.3 nM). Furthermore, decreasing doses of PLN induced TF expression in HPMCs, with the lowest dose of PLN (0.3 nM) inducing TF protein to the greatest extent.

Because TF protein and mRNA were increased by FXa, THB, PLN, and uPA, TF surface activity was assayed in HPMCs using an FX activation assay. Surface TF activity was found to be increased in FXa-, THB-, PLN-, and uPA-treated HPMCs compared with PBS controls (Figure 7F). Conversely, TGF-β–treated cells showed no change in surface TF activity in this analysis. These findings demonstrate that the coagulation proteases, FXa and THB, as well as uPA and PLN, are capable of inducing TF activity in PMCs, suggesting that unrestricted uPA or PLN, and feed-forward stimulation by FXa or THB could potentiate the mesothelial procoagulant response associated with CBB-induced pleural injury in PAI-1–deficient mice.

Discussion

This study addresses two objectives. The first is the adaptation of the CBB model, which closely recapitulates the morphologic and pathophysiologic derangements observed in human fibrothoraces, to the C57BL/6j mouse. The CBB pleural injury model in CD1 mice was originally reported by DeCologne and colleagues (10), and extension to C57BL/6j mice enabled the use of genetically manipulated mice developed in this line. The second is elucidation of the role of PAI-1 and disordered fibrin turnover in the progression of morphologic and physiologic derangements associated with CBB-induced pleural injury. Although the use of fibrinolytic agents, such as tissue type PA or uPA, are currently accepted treatments for organizing pleural injury, the role of their primary inhibitor, PAI-1, in the pathogenesis of pleuritis-associated lung restriction has been poorly understood (25). This study shows that PAI-1 is essential for

Figure 4. (Continued). Intrapleural administration of CBB alters pulmonary function and lung architecture. Pulmonary function tests and CT scans were performed on wild-type (WT), plasminogen activator inhibitor (PAI)-1$^{-/-}$, and PAI-1 transgenic (PAI-1^{Tg}) mice 14 days after intrapleural injection with saline or CBB. Pulmonary function measurements were taken using the flexiVent system. Lung volumes were calculated from CT scan renditions. (*A*) CBB-injured mice demonstrated significantly lower lung volumes than similarly treated WT and PAI-1$^{-/-}$ mice. There was no significant difference in lung volumes between saline- and CBB-injured PAI-1^{Tg} mice. PAI-1$^{-/-}$ mice with CBB-induced pleural injury had significantly lower lung volumes compared with similarly treated WT and PAI-1^{Tg} mice. PAI-1$^{-/-}$ mice exhibited significantly increased resistance (*B*) and elastance (*C*) compared with similarly treated CBB-injured WT and PAI-1^{Tg} mice. (*D*) CBB-injured PAI-1$^{-/-}$ mice had significantly lower dynamic lung compliance than WT and PAI-1^{Tg} mice. (*E*) Tissue sections from saline- and CBB-treated WT, PAI-1$^{-/-}$, and PAI-1^{Tg} mice were Trichrome stained to detect collagen deposition (*blue*). CBB-injured PAI-1$^{-/-}$ mice exhibited increased collagen deposition in the subpleural mesothelium when compared with similarly treated WT and PAI-1^{Tg} mice. Pleural thicknesses from stained lung sections were measured and collected from 30 fields per slide (n = 3 representative sections per group). CBB-injured PAI-1$^{-/-}$ mice exhibited significantly thicker pleura than WT and PAI-1^{Tg} mice 14 days after CBB administration (*$P < 0.05$). (*F*) The sections were probed for fibrin(ogen) deposition by immunohistochemistry at the level of the pleural and subpleural mesothelium by light microscopy. (*G*) Fibrin(ogen) deposition was the most abundant in the PAI-1^{Tg} animals, and was significantly increased compared with WT and PAI-1$^{-/-}$ mice 14 days after CBB injury. Fibrin thickness from stained lung sections were measured and collected from 30 fields per slide (n = 3 representative sections per group). Data shown are means ± SEM (*$P < 0.05$).

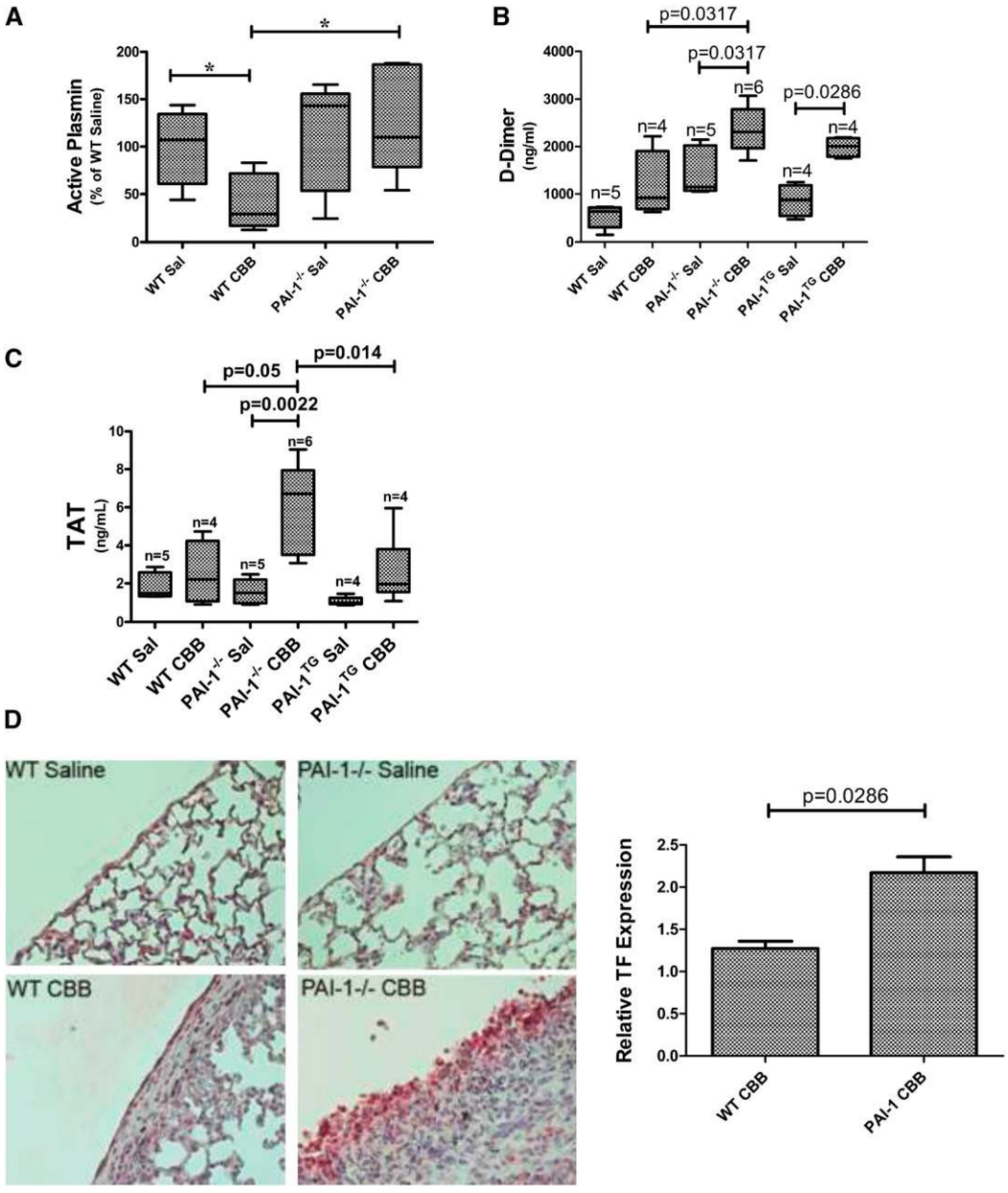

Figure 5. Active plasmin (PLN), D-dimers, and thrombin–antithrombin (TAT) complexes are increased in pleural lavage of CBB-injured PAI-$1^{-/-}$ mice. Pleural lavages were collected from WT, PAI-$1^{-/-}$, and PAI-1^{Tg} mice 14 days after intrapleural administration of saline or CBB. Pleural lavages were assayed for active PLN (*A*), D-dimers (*B*), and TAT complexes (*C*) by ELISA. (*A*) Active PLN was elevated in CBB-injured PAI-$1^{-/-}$, while being significantly reduced in similarly treated WT mice compared with saline control animals. CBB-injured PAI-$1^{-/-}$ mice exhibited significantly higher active PLN levels than similarly treated WT mice (n = 4–6 mice/group; *$P < 0.05$). (*B*) D-dimers were elevated in CBB-injured mice from each group. CBB-injured PAI-$1^{-/-}$ mice exhibited significantly higher D-dimer levels than similarly treated WT mice. (*C*) TAT complexes were elevated in the pleural lavages of CBB-injured mice from each group. CBB-injured PAI-$1^{-/-}$ mice exhibited significantly higher TAT complex levels than similarly treated WT and PAI-1^{Tg} mice (n = 4–6 mice/group). (*D*) Tissue factor (TF) expression was significantly greater in CBB-injured PAI-$1^{-/-}$ mice when compared with similarly treated WT animals (n = 4/group). TF levels were determined on the basis of relative intensity of TF staining (*red stain*) and evaluated using a 5-point scale (30 fields/section for each of 4 mice/group were visualized to determine TF antigen levels). Data shown are means ± SEM.

appropriate resolution of pleural injury, and that its deficiency paradoxically exacerbates CBB-induced pleural fibrosis with restrictive pathophysiologic consequences. These changes are fostered by cross-talk with procoagulants within exudative pleural fluids and unrestricted uPA and PLN activity that collectively promote mesenchymal transition of PMCs lining the visceral pleura.

Although bleomycin has long been used to induce fibrosis in mice, we report here that the combination of carbon black nanoparticles and bleomycin, CBB, potently induces pleural fibrosis in C57Bl/6j mice. In a follow-up time course analysis, CBB injury negatively impacted lung function (total lung resistance, elastance, and compliance)

and lung volume as early as 2 days after injury, and trends of worsened lung function were apparent over the subsequent 21 days. Although CBB-injury was characterized by early fibrin deposition (2 d), collagen became the dominant ECM protein in the thickened pleural rind as the injury progressed (7–21 d). The presence of increasing collagen, pleural thickening, and visceral fibrin deposition observed in the CBB model closely recapitulates features we discovered to be associated with human pleuritis.

In confocal microscopy studies, the colocalization of calretinin, a mesothelial cell marker, with α-SMA, a myofibroblast marker, show that MesoMT contributes to the pool of myofibroblasts associated with pleural thickening associated with CBB injury. Parenchymal migration of myofibroblasts (best seen in Figure 6) was observed in the CBB model, consistent with that observed in TGF-β–induced pleural remodeling (11). Our data show that MesoMT likewise contributes to pleural thickening associated with human pleuritis and CBB-mediated pleural injury. Other sources of myofibroblasts, including lung epithelial cells, fibroblasts, or fibrocytes within the lung parenchyma, may also be represented. A limitation of this study is the lack of a fate-mapping approach in which the progression of MesoMT can be followed in labeled mesothelial cells, but flow cytometry clearly showed that the vast majority of α-SMA–expressing cells isolated from pleural lavage of the injured pleural space were of mesothelial origin in the CBB mouse model. These findings strongly support our hypothesis that resident PMCs are a major source of myofibroblasts seen in the visceral pleura in the CBB pleural injury model.

Our data show that resident mesothelial cells can undergo MesoMT, and that these cells appear to contribute to the pool of pleural myofibroblasts associated with CBB injury. Furthermore, a correlation between higher numbers of α-SMA–expressing myofibroblasts in PAI-$1^{-/-}$ mice and restrictive lung disease was observed in these studies. However, tissue remodeling in CBB-induced pleural injury involves other processes that may contribute to pleural organization and lung restriction. Active TGF-β is detectable in pleural lavage of mice with CBB-induced lung injury, but significant increments or incremental trends were not found in pleural lavage at the intervals we studied after induction of pleural injury by CBB. CBB injury is also characterized by excess fibrin and collagen deposition in the pleural space at the visceral pleural surface, which is increased in PAI-1–deficient mice. Although the relative contributions of these processes to pathophysiologic changes in lung function are currently unknown, all appear to contribute to the restrictive changes associated with CBB-induced pleural injury.

To assess the role of PAI-1 and protracted aberrant fibrinolysis in the progression of CBB-induced pleural injury, we compared injury outcomes by gross examination, CT imaging, morphometry, and pulmonary function testing in WT, PAI-1–deficient, and PAI-1–overexpressing mice. Although CBB caused significant injury in each group, the PAI-$1^{-/-}$ mice consistently demonstrated significantly worse pleural injury and greater restrictive pathophysiologic changes than WT and PAI-1^{Tg} mice 14 days after injury. Furthermore, CBB-injured PAI-$1^{-/-}$ mice exhibited notable respiratory distress by 14 days, and became moribund by 21 days, whereas CBB-injured WT mouse behavior was similar to that of the saline control animals. PAI-1^{Tg} mice displayed increased pleural fibrin(ogen) deposition in the visceral pleural tissues, and fibrin strands were found in the pleural space. Although CBB-injured PAI-1^{Tg} mice exhibited significant differences in resistance, elastance, and compliance, lung volumes were not significantly decreased compared with WT mice. Visceral pleural thickening was apparent in CBB-injured PAI-1^{TG} mice, but pleural collagen deposition was not as robust compared with similarly treated PAI-$1^{-/-}$ mice. These findings indicate that fibroproliferation and collagen deposition characterize and promote CBB-induced restrictive lung disease. Furthermore, we present the novel use of pulmonary function testing and lung volume determinations as reliable indices of pleural organization and thickening in this model.

The fibrin strands found in the CBB-injured PAI-1^{Tg} mice were modest compared

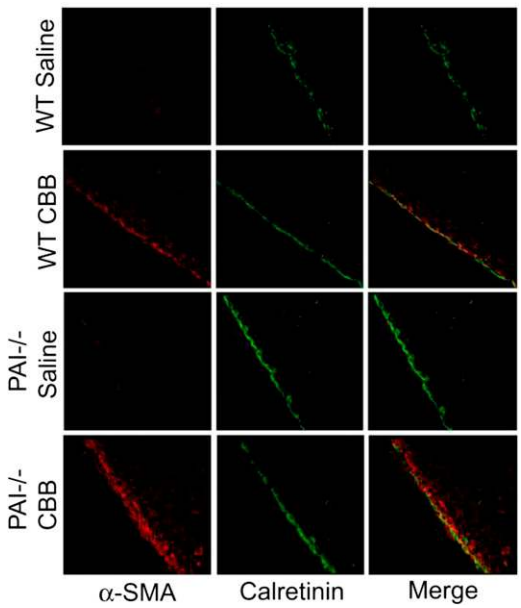

Figure 6. PAI-1 deficiency contributes to increased α-SMA expression and colocalization with calretinin by the pleural and subpleural mesothelium in CBB-induced pleural injury. Tissue sections were prepared from the lungs of saline- and CBB-treated WT and PAI-$1^{-/-}$ mice 14 days after intrapleural injection (n = 3/group). The sections were then probed for the expression of α-SMA and calretinin at the level of pleural and subpleural mesothelium by confocal microscopy. The pleural and subpleural mesothelium in its entirety was analyzed for α-SMA (*red*) and calretinin (*green*) expression and colocalization. Increased α-SMA and calretinin colocalization was observed in CBB-treated PAI-$1^{-/-}$ mice compared with similarly treated WT mice. All images were taken at 40× magnification on a confocal microscope (30 fields/section for each of 3 mice/group were visualized to determine α-SMA and calretinin expression; images illustrate representative findings from these analyses).

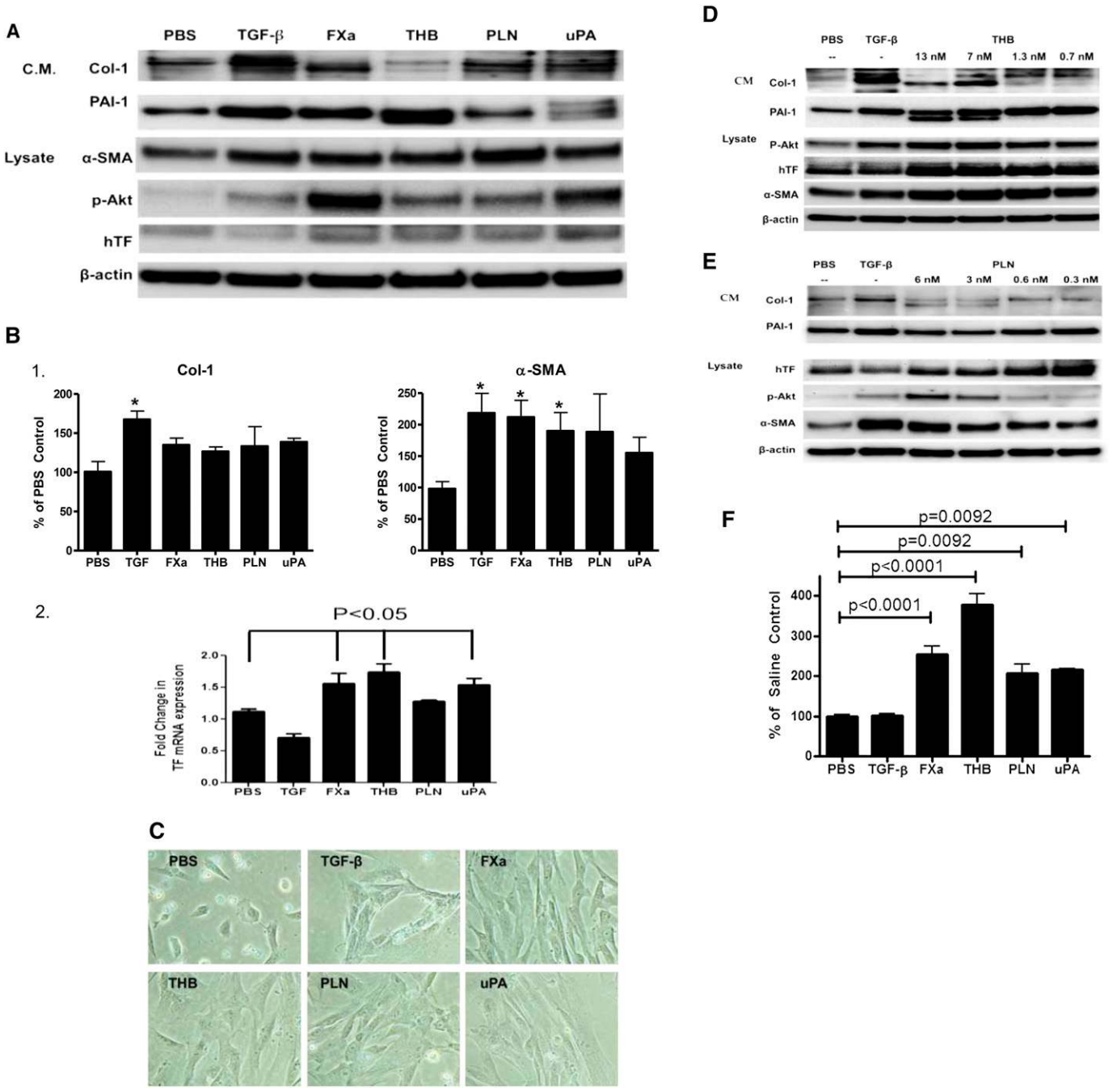

Figure 7. Coagulation cascade proteases and fibrinolytic pathway components induce mesothelial–mesenchymal transition (MesoMT) in pleural mesothelial cells (PMCs). Serum-starved human PMCs (HPMCs) (*A–C*) were treated with PBS, transforming growth factor (TGF)-β (5 ng/ml), factor Xa (FXa; 20 nm), thrombin (THB; 13 nM), PLN (6 nM), and two-chain urokinase plasminogen activator (tc-uPA; 20 nM). (*A*) HPMC cell lysates (5 μg) and conditioned medias (40 μl) were resolved by SDS-PAGE and analyzed via Western blot for markers of MesoMT: collagen (Col)-1, PAI-1, α-SMA, and p-Akt. HPMC lysates were also probed for TF. β-actin was used as a loading control. (*B*) RNA from treated HPMCs was transcribed into cDNA. *Panel 1*: Col-1 and α-SMA mRNA expression in HPMCs were also analyzed by PCR. Densitometry was performed on the resolved bands and standardized to glyceraldehyde 3-phosphate dehydrogenase (GAPDH). *Panel 2*: TF expression was analyzed by quantitative PCR with GAPDH expression used as a normalization control (*$P < 0.05$). (*C*) HPMCs were treated with PBS, TGF-β, FXa, THB, PLN, and uPA for 48 hours. Cells were then imaged using phase contract microscopy. Images are representative of three independent experiments. (*D*) HPMCs were treated with PBS, TGF-β (positive control), and a decreasing range of THB (13–0.7 nM). Lysates (5 μg) and conditioned media (40 μl) were resolved by SDS-PAGE and probed for Col-1, PAI-1, p-Akt, TF, and α-SMA. (*E*) HPMCs were treated with PBS, TGF-β, and a decreasing range of PLN (6–0.3 nM). Lysates (5 μg) and conditioned media (40 μl) were resolved by SDS-PAGE and probed for Col-1, PAI-1, p-Akt, TF, and α-SMA. β-actin was used as a loading control. (*F*) HPMCs were treated with PBS, TGF-β, FXa, THB, PLN, and uPA, and assayed for surface TF activity using an FX conversion assay. FXa, THB, uPA, and PLN increased surface TF activity in HPMCs ($n \geq 3$/group). Data shown are means ± SEM. CM, conditioned media.

Table 1: Forward and Reverse Primer Sequences and Origins

Target	Sequence
Human Col-1 Fw	GAACGCGTGTCATCCCTTGT
Human Col-1 Rev	GAACGAGGTAGTCTTTCAGCAACA
Human α-SMA Fw	CGTTACTACTGCTGAGCGTGA
Human α-SMA Rev	AACGTTCATTTCCGATGGTG
Human TF Fw	ACGCTCCTGCTCGGCTGGGT
Human TF Rev	CGTCTGCTTCACATCCTTCA
Human GAPDH Fw	ACCACAGTCCATGCCATCAC
Human GAPDH Rev	TCCACCACCCTGTTGCTGTA

Definition of abbreviations: α-SMA, α-smooth muscle actin; Col, collagen; Fw, forward; GAPDH, glyceraldehyde 3-phosphate dehydrogenase; Rev, reverse; TF, tissue factor.

with the findings in tetracycline-induced injury in rabbits (26, 27), suggesting that analyses over later intervals would be unlikely to yield pleurodesis or worse restriction. Indeed, we could not generate pleural injury in C57Bl/6j mice using intrapleural tetracycline, talc, or silver nitrate (data not shown), so we infer that C57Bl/6j mice resist these forms of pleural injury. The resistance to pleural injury is likely why the combination of carbon black with bleomycin is necessary to generate the model, as we found that intrapleural administration of either bleomycin or carbon black alone did not induce pleural injury.

The finding that CBB induced more robust, accelerated pleural restriction in PAI-$1^{-/-}$ mice is in contrast to previously published work focused on accelerated pulmonary fibrosis, in which PAI-1 deficiency ameliorated bleomycin-induced lung injury in mice (28, 29). There are two principle differences between those reports and the present study. First, bleomycin in combination with carbon black was used to initiate pleural injury, and, second, the profibrogenic stimulus was administered intrapleurally. Consistent with the findings we now report, Hertig and colleagues (30) reported that PAI-1 deficiency exacerbated fibrosis in a glomerular nephritis mouse model. Our findings are also consistent with those in cardiac injury, in which incremental uPA or decremental PAI-1 fosters cardiac fibrosis (31, 32). Our data indicate that PAI-1 deficiency potentiates CBB-mediated pleural injury by exacerbating visceral pleural organization sufficient to worsen lung restriction.

In addition to the significantly worse physiological changes in CBB-injured PAI-1–deficient mice, active PLN, TAT complexes, and D-dimer levels were concurrently increased in the pleural lavages of PAI-1–deficient animals when compared with similarly treated WT mice. The findings indicate that local, protracted (over 21 d) elaboration of increased PLN activity could contribute to mesenchymal transition and increased organization of the mesothelium in PAI-$1^{-/-}$ mice. TAT and D-dimer ELISA analyses were performed, because enzyme activity levels (FXa and uPA, respectively) were below detectable levels in our analyses. These findings strongly suggest that cross-talk between an augmented procoagulant response and unrestricted uPA and PLN occurred in CBB-injured PAI-$1^{-/-}$ mice. Although D-dimer concentrations were elevated in PAI-1^{Tg} mice, these findings are likely due to the significantly higher amounts of fibrin(ogen) found in the CBB-injured PAI-1^{Tg} mouse. Our data show that the pleural lavage procoagulant response is attributable in part to uPA/PLN–induced TF in PMCs, an effect that appears to be recapitulated by procoagulants generated in pleural injury. These observations suggest a novel mechanism of uPA and PLN-mediated regulation of coagulation cascade proteases and mesothelial procoagulant responses that promotes increased pleural organization and lung restriction.

We here report the novel finding that coagulation cascade and fibrinolytic proteases induce MesoMT in human and mouse PMCS. In addition, subnanomolar quantities of PLN and THB (600 and 700 pM, respectively) were found to induce markers of MesoMT. Although the highest THB concentration (13 nM) was not found to induce collagen at the protein level, THB did increase Col-1 mRNA, suggesting that col-1 is extensively cleaved at the highest concentration of THB used in this study. Supporting this interpretation, it has previously been reported that THB at high levels promotes collagen degradation through an indirect mechanism (33). Although it has been shown previously that FXa and THB can induce TF expression, we now show, for the first time, that fibrinolytic proteases enhance TF expression. Specifically, uPA and PLN enhance TF expression and activity in PMCs. These findings, and the increased TAT complexes in pleural lavage of PAI-$1^{-/-}$ mice, indicate that increased uPA and PLN activity accompanies PAI-1 deficiency, contributes to increased coagulation cascade activity, and increases the extent of pleural organization.

Finally, this study demonstrates that coagulation cascade and fibrinolytic proteases induce MesoMT *in vitro*, and could contribute to CBB-induced pleural fibrosis *in vivo*. Furthermore, these findings strongly support the notion that cross-talk exists between these pathways *in vivo*. Treatment strategies in which PAI-1 is a therapeutic target will need to preserve enough PAI-1 activity to limit the possibility of florid visceral pleural thickening. Current therapies that employ fibrinolytics do not completely deplete PAI-1, which is continuously renewed in pleural injury through elaboration by the mesothelium and other resident cell populations and extravasation resulting from increased vascular permeability. Although PAI-1 can limit the successful use of fibrinolytics in the treatment of pleural loculation and fibrosis, the presence of PAI-1 in the pleural compartment appears to be required to limit the development of CBB-induced visceral pleural thickening and restrictive lung dysfunction. ■

Author disclosures are available with the text of this article at www.atsjournals.org.

References

1. Jantz MA, Antony VB. Pleural fibrosis. *Clin Chest Med* 2006;27:181–191.
2. Heffner JE, Klein JS, Hampson C. Interventional management of pleural infections. *Chest* 2009;136:1148–1159.
3. Corcoran JP, Hallifax R, Rahman NM. New therapeutic approaches to pleural infection. *Curr Opin Infect Dis* 2013;26:196–202.
4. Idell S. The pathogenesis of pleural space loculation and fibrosis. *Curr Opin Pulm Med* 2008;14:310–315.

5. Idell S, Koenig KB, Fair DS, Martin TR, McLarty J, Maunder RJ. Serial abnormalities of fibrin turnover in evolving adult respiratory distress syndrome. *Am J Physiol* 1991;261:L240–L248.
6. Zhang YP, Li WB, Wang WL, Liu J, Song SX, Bai LL, Hu YY, Yuan YD, Zhang M. siRNA against PLNogen activator inhibitor-1 ameliorates bleomycin-induced lung fibrosis in rats. *Acta Pharmacol Sin* 2012;33: 897–908.
7. Osterholzer JJ, Christensen PJ, Lama V, Horowitz JC, Hattori N, Subbotina N, Cunningham A, Lin Y, Murdock BJ, Morey RE, *et al*. PAI-1 promotes the accumulation of exudate macrophages and worsens pulmonary fibrosis following type II alveolar epithelial cell injury. *J Pathol* 2012;228:170–180.
8. Swaisgood CM, French EL, Noga C, Simon RH, Ploplis VA. The development of bleomycin-induced pulmonary fibrosis in mice deficient for components of the fibrinolytic system. *Am J Pathol* 2000; 157:177–187.
9. Karandashova S, Florova G, Azghani AO, Komissarov AA, Koenig K, Tucker TA, Allen TC, Stewart K, Tvinnereim A, Idell S. Intrapleural adenoviral delivery of human PLNogen activator inhibitor-1 exacerbates tetracycline-induced pleural injury in rabbits. *Am J Respir Cell Mol Biol* 2013;48:44–52.
10. DeCologne N, Wettstein G, Kolb M, Margetts P, Garrido C, Camus P, Bonniaud P. Bleomycin induces pleural and subpleural fibrosis in the presence of carbon particles. *Eur Respir J* 2010;35:176–185.
11. Decologne N, Kolb M, Margetts PJ, Menetrier F, Artur Y, Garrido C, Gauldie J, Camus P, Bonniaud P. TGF-beta1 induces progressive pleural scarring and subpleural fibrosis. *J Immunol* 2007;179: 6043–6051.
12. Kalluri R, Neilson EG. Epithelial–mesenchymal transition and its implications for fibrosis. *J Clin Invest* 2003;112:1776–1784.
13. Nasreen N, Mohammed KA, Mubarak KK, Baz MA, Akindipe OA, Fernandez-Bussy S, Antony VB. Pleural mesothelial cell transformation into myofibroblasts and haptotactic migration in response to TGF-beta1 *in vitro*. *Am J Physiol* 2009;297:L115–L124.
14. Ando S, Otani H, Yagi Y, Kawai K, Araki H, Fukuhara S, Inagaki C. Proteinase-activated receptor 4 stimulation–induced epithelial–mesenchymal transition in alveolar epithelial cells. *Respir Res* 2007;8:31.
15. Scotton CJ, Krupiczojc MA, Konigshoff M, Mercer PF, Lee YC, Kaminski N, Morser J, Post JM, Maher TM, Nicholson AG, *et al*. Increased local expression of coagulation factor X contributes to the fibrotic response in human and murine lung injury. *J Clin Invest* 2009; 119:2550–2563.
16. Glauser FL, Otis PT, Levine RI, Smith WR. Coagulation factors and fibrinogen in pleural effusions. *Respiration* 1976;33:396–402.
17. Mutsaers SE, Prele CM, Brody AR, Idell S. Pathogenesis of pleural fibrosis. *Respirology* 2004;9:428–440.
18. Williams L, Tucker TA, Koenig K, Allen T, Rao LV, Pendurthi U, Idell S. Tissue factor pathway inhibitor attenuates the progression of malignant pleural mesothelioma in nude mice. *Am J Respir Cell Mol Biol* 2012;46:173–179.
19. Lugli A, Forster Y, Haas P, Nocito A, Bucher C, Bissig H, Mirlacher M, Storz M, Mihatsch MJ, Sauter G. Calretinin expression in human normal and neoplastic tissues: a tissue microarray analysis on 5233 tissue samples. *Hum Pathol* 2003;34:994–1000.
20. Ma J, Weisberg A, Griffin JP, Vaughan DE, Fogo AB, Brown NJ. PLNogen activator inhibitor-1 deficiency protects against aldosterone-induced glomerular injury. *Kidney Int* 2006;69: 1064–1072.
21. Khalil N, Corne S, Whitman C, Yacyshyn H. Plasmin regulates the activation of cell-associated latent TGF-beta 1 secreted by rat alveolar macrophages after *in vivo* bleomycin injury. *Am J Respir Cell Mol Biol* 1996;15:252–259.
22. Koh TJ, Bryer SC, Pucci AM, Sisson TH. Mice deficient in PLNogen activator inhibitor-1 have improved skeletal muscle regeneration. *Am J Physiol Cell Physiol* 2005;289:C217–C223.
23. Chuang-Tsai S, Sisson TH, Hattori N, Tsai CG, Subbotina NM, Hanson KE, Simon RH. Reduction in fibrotic tissue formation in mice genetically deficient in PLNogen activator inhibitor-1. *Am J Pathol* 2003;163:445–452.
24. Patel P, Sekiguchi Y, Oh KH, Patterson SE, Kolb MR, Margetts PJ. Smad3-dependent and -independent pathways are involved in peritoneal membrane injury. *Kidney Int* 2010;77:319–328.
25. Tucker T, Idell S. PLNogen–PLN system in the pathogenesis and treatment of lung and pleural injury. *Semin Thromb Hemost* 2013;39: 373–381.
26. Idell S, Allen T, Chen S, Koenig K, Mazar A, Azghani A. Intrapleural activation, processing, efficacy, and duration of protection of single-chain urokinase in evolving tetracycline-induced pleural injury in rabbits. *Am J Physiol* 2007;292:L25–L32.
27. Idell S, Mazar A, Cines D, Kuo A, Parry G, Gawlak S, Juarez J, Koenig K, Azghani A, Hadden W, *et al*. Single-chain urokinase alone or complexed to its receptor in tetracycline-induced pleuritis in rabbits. *Am J Respir Crit Care Med* 2002;166:920–926.
28. Eitzman DT, McCoy RD, Zheng X, Fay WP, Shen T, Ginsburg D, Simon RH. Bleomycin-induced pulmonary fibrosis in transgenic mice that either lack or overexpress the murine PLNogen activator inhibitor-1 gene. *J Clin Invest* 1996;97:232–237.
29. Hattori N, Degen JL, Sisson TH, Liu H, Moore BB, Pandrangi RG, Simon RH, Drew AF. Bleomycin-induced pulmonary fibrosis in fibrinogen-null mice. *J Clin Invest* 2000;106:1341–1350.
30. Hertig A, Berrou J, Allory Y, Breton L, Commo F, Costa De Beauregard MA, Carmeliet P, Rondeau E. Type 1 PLNogen activator inhibitor deficiency aggravates the course of experimental glomerulonephritis through overactivation of transforming growth factor beta. *FASEB J* 2003;17:1904–1906.
31. Ghosh AK, Bradham WS, Gleaves LA, De Taeye B, Murphy SB, Covington JW, Vaughan DE. Genetic deficiency of PLNogen activator inhibitor-1 promotes cardiac fibrosis in aged mice: involvement of constitutive transforming growth factor-beta signaling and endothelial-to-mesenchymal transition. *Circulation* 2010;122:1200–1209.
32. Stempien-Otero A, Plawman A, Meznarich J, Dyamenahalli T, Otsuka G, Dichek DA. Mechanisms of cardiac fibrosis induced by urokinase PLNogen activator. *J Biol Chem* 2006;281:15345–15351.
33. Galis ZS, Kranzhofer R, Fenton JW , II, Libby P. Thrombin promotes activation of matrix metalloproteinase-2 produced by cultured vascular smooth muscle cells. *Arterioscler Thromb Vasc Biol* 1997; 17:483–489.